Nanoscale

COMMUNICATION

View Article Online
View Journal | View Issue

Cite this: *Nanoscale*, 2016, **8**, 12524

Received 29th November 2015,
Accepted 7th January 2016

DOI: 10.1039/c5nr08463f

www.rsc.org/nanoscale

Improving nanoparticle diffusion through tumor collagen matrix by photo-thermal gold nanorods†

Vahid Raeesi[a,b] and Warren C. W. Chan*[a,b,c,d]

Collagen (I) impairs the targeting of nanoparticles to tumor cells by obstructing their diffusion inside dense tumor interstitial matrix. This potentially makes large nanoparticles (>50 nm) reside near the tumor vessels and thereby compromises their functionality. Here we propose a strategy to locally improve nanoparticle transport inside collagen (I) component of the tumor tissue. We first used heat generating gold nanorods to alter collagen (I) matrix by local temperature elevation. We then explored this impact on the transport of 50 nm and 120 nm inorganic nanoparticles inside collagen (I). We demonstrated an increase in average diffusivity of 50 nm and 120 nm in the denatured collagen (I) by ~14 and ~21 fold, respectively, compared to intact untreated collagen (I) matrix. This study shows how nanoparticle-mediated hyperthermia inside tumor tissue can improve the transport of large nanoparticles through collagen (I) matrix. The ability to increase nanoparticles diffusion inside tumor stroma allows their targeting or other functionalities to take effect, thereby significantly improving cancer therapeutic or diagnostic outcome.

A major focus in cancer nanomedicine is to transport nanoparticles to cells within tumor milieu.[1–3] Nanoparticles are designed as imaging probes[4–6] and therapeutic agents[7–10] to target tumor cells. Nanoparticles are surface modified with a ligand that is specifically recognized by tumor cells[11,12] and are then injected into the bloodstream. These nanoparticles are next transported through blood circulation to the tumor vessels, where it has been proposed they escape the leaky tumor vessels *via* leaky vessels.[13–15] Once nanoparticles cross the vessel wall, they need to be transported through the tumor interstitial matrix to reach the cells. Collagen (I), a major protein in the tumor interstitium,[16] forms a dense 3D network of fibrilar structure in the interstitial space between the tumor cells and blood vessels, and acts as one of the dominant physiological barrier against diffusion inside the tumor.[17–19] This poses a great challenge for many nanoparticle designs, especially for larger sizes (*e.g.*, 100 nm) that get stuck within the collagen network.[20] If the nanoparticles are unable to diffuse through the tumor interstitial matrix, they will reside near the vessel. There are two consequences to this: (1) targeted nanoparticles will not be able to interact with receptors on the cells, and (2) tumor retention may be shortened as they can easily diffuse out of the tumor because of high interstitial pressure (IFP).[21] The inability of nanoparticles to transport through the tumor interstitial matrix may be a reason that a number of recent studies showed a lack of difference in total tumor accumulation between active and passive-design nanoparticles.[22–25] Hence, there is a need to develop strategies to alter the tumor matrix to enable transport of nanoparticles through it. A number of strategies have been proposed: (a) the use and incorporation of proteolytic enzyme collagenase[26] in the nanoparticle design[27–29] and (b) design of larger nanoparticles to degrade and release smaller nanoparticles within the tumor matrix.[30] However, these strategies have limitations. First, free collagenase can not be systematically administered as collagen is the structural protein in other organs[31] or it may lose activity during nanoparticle formulation process.[32] Second, conversion of large particle assemblies to small nanoparticles require intricate design chemistry to minimize degradation during circulation[33] and rapid release[34] within tumor matrix before being cleared by elevated IFP.[35] Given the heterogeneity of tumors plus variable tumor retention rates based on nanoparticle physical-chemical properties, it may be difficult to design a unified nanosystem for this purpose.

Here we proposed a strategy to locally improve nanoparticle transport through collagen (I) component of the tumor tissue. In a collagen (I) μ-channel setup, we first introduced gold nanorods (GNRs) to alter the collagen (I) matrix under near-infrared (NIR) light stimulation. We showed local irreversible denaturation of collagen (I) fibrils by using GNRs to photo-

[a]*Department of Material Science and Engineering, University of Toronto, Toronto M5S 3E1, Canada. E-mail: warren.chan@utoronto.ca*
[b]*Institute of Biomaterials and Biomedical Engineering, University of Toronto, Toronto, Ontario M5S 3G9, Canada*
[c]*Department of Chemical Engineering Toronto, University of Toronto, Toronto, Ontario M5S 3E5, Canada*
[d]*Department of Chemistry, University of Toronto, Toronto, Ontario M5S 3H6, Canada*

†Electronic supplementary information (ESI) available. See DOI: 10.1039/c5nr08463f

thermally increase the local temperature to 45–55 °C. We then introduced two sizes of 50 nm and 120 nm nanoparticles with the same surface chemistry into both treated and untreated collagen (I) μ-channels. We demonstrated an increase in average diffusivity of 50 nm and 120 nm in the denatured collagen (I) by ~14 and ~21 fold, respectively, compared to intact untreated collagen (I) matrix. This study shows how nanoparticle-mediated hyperthermia inside tumor tissue can improve the transport of large nanoparticles (>50 nm) through collagen (I) matrix.

GNRs were selected for this study because the heat generated by these nanoparticles have a theoretical photo-thermal (PTT) conversion efficiency of >90% with NIR wavelength excitation between 700–850 nm. Also, this wavelength range has been shown to yield the largest tissue penetration depth.[36] GNRs have been applied in cancer therapy as a hyperthermia agent[37–40] or as part of a combinatorial strategy for synergistic killing[41–43] of tumor cells. The experimental set-up to study the effect of GNRs generated heat on transport through a collagen (I) matrix is described in Fig. 1a and b. The glass μ-chip

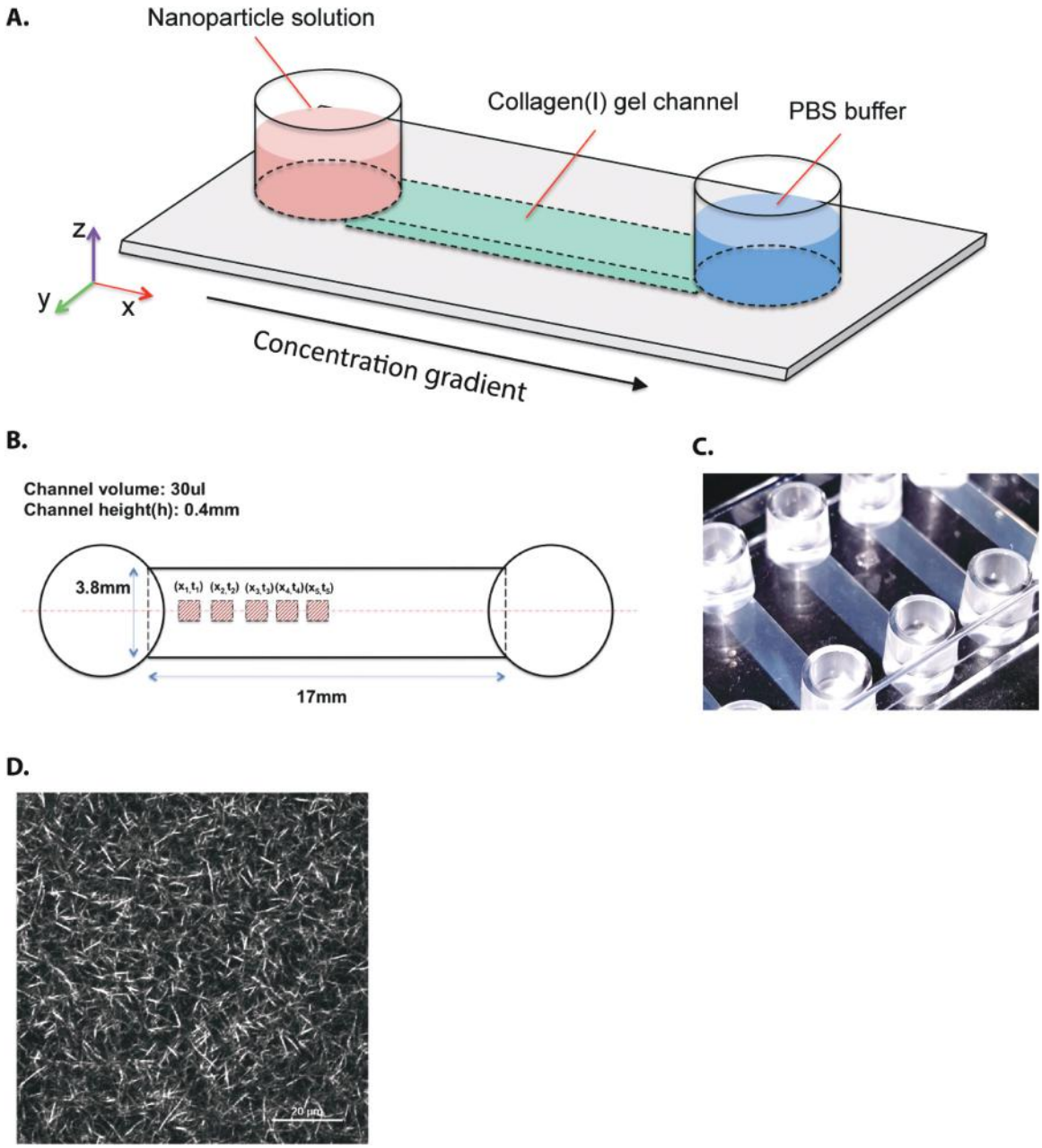

Fig. 1 Design of the tumor collagen (I) matrix barrier model. (A) Schematic of the μ-chip design. (B) *XY*-plane projection of the μ-channel: the μ-channel dimensions are 17 mm × 3.8 mm × 0.4 mm (*L* × *W* × *H*), which can accommodate 30 μl collagen (I) hydrogel. The thin glass slide at the bottom would enable imaging by confocal fluorescence microscopy along the μ-channel. (C) Optical image of the μ-channels filled with intact collagen (I) proteins between the reservoirs appear turbid. (D) Reflectance confocal image of the collagen (I) matrix at 7 mg ml^{-1} concentration inside a μ-channel.

had two reservoirs, which were connected through a μ-channel. We filled the channel with bovine collagen (I) solution and neutralized it to form a rigid gel structure in 4 h. The collagen (I) matrix appeared turbid inside the μ-channel (Fig. 1c). Reflectance confocal imaging revealed a porous structure with randomly oriented collagen fibers at a concentration ranging from 2–7 mg mL^{-1} (Fig. S1†). A 7 mg ml^{-1} collagen concentration (Fig. 1d) was used for the rest of the experiments as it was in the range of the reported collagen (I) contents in tumors.[44] The transport mode in our setup was diffusion (derived by concentration gradient) as there was no convective flow (Peclet number ~0). GNRs were synthesized *via* a directional growth of gold seeds in cetyltrimethyl ammonium bromide (CTAB) surfactant and ascorbic acid[41,45] (see Materials and methods in the ESI†). Next, GNRs were coated with polyethylene glycol (PEG) to stabilize them in a buffer medium. The GNRs had an average length to width ratio of 28 nm × 7 nm (Fig. 2a), longitudinal absorption peak at 740 nm and a transverse peak at 520 nm (Fig. 2b). 30 μl GNRs were added to one reservoir and the other reservoir was filled with equal volume of phosphate buffered saline (PBS). Then we used a continuous wavelength near-IR laser (785 nm) to excite the GNRs and the temperature was monitored using thermal imaging. We first correlated the relationship between GNR concentration and laser power to control temperature elevation (Fig. 2c and S2†). We utilized this characterization to study the effect of heat on collagen (I) gel structure in the μ-channels. We raster irradiated the channel horizontally with a 5 mm diameter laser beam in one side of the μ-channel. We optimized the GNR concentration (6 nM), laser power density (3 W cm^{-2}) so that the channel exposed-area exhibit an average temperature between 45–55 °C, in the range of reported collagen (I) denaturation temperatures[46,47] (see Fig. 2d). When the μ-channel was heated, the exposed area became clear. The heated medium converted from a dense hydrogel to a liquid-like medium. We detected no reflectance signal from collagen fibrils in the photo-thermally exposed area (Fig. 2e and f) with 88% loss of turbidity (as measured by absorbance measurements at 405 nm (ref. 48)) compared to non-exposed areas (Fig. 2g), suggesting the disappearance of collagen fibers. After cooling, the fiber structure did not re-form, indicating irreversible denaturation of collagen fibers. This is likely due to the transformation of the native triple helical structure into a random coiled structure as reported by previous studies.[49] This change in conformation was further confirmed by the observation of agglomerates at the bottom of the channel wall (Fig. 2h).

The GNR's PTT experiments clearly showed that the fibrilar structure was altered in the collagen (I) matrix. We next evaluated whether this change in collagen (I) matrix would lead to an increase in transport of spherical nanoparticles. We selected gold nanoparticles of 50 and 120 nm core diameters as model particle systems. These spherical gold nanoparticles were synthesized using a hydroquinone-seed mediated growth method and surface coated with polyethylene glycol and AlexaFluor dye molecules using the previous developed methods from our laboratory (Fig. 3a, see Materials and methods†). This dye was selected because it can be excited at 647 nm and the emission is far from the plasmon band of the gold nanoparticles, so that minimal quenching of the dye by gold nanoparticle surface would occur. The 50 nm and 120 nm nanoparticles showed plasmon peaks at 535 nm and 595 nm, respectively (Fig. 3b). TEM images revealed their size and shape with narrow size distribution (Fig. S3†) and this was supported by dynamic light scattering measurements with a PDI < 0.06.

To demonstrate GNR's PTT effect on diffusion, we added GNRs (6 nM) in one reservoir of both μ-channels and then illuminated the channel with a laser for 6 min using our previously optimized conditions. We then added the fluorescently-tagged nanoparticles on top of the GNRs reservoir and then traced the motion of the nanoparticles as they were diffusing along the collagen (I) matrix channel length using confocal fluorescence microscopy (Materials and Methods). Images were recorded in 12 h at different distances along the μ-channel and processed using ImageJ and Matlab to develop spatio-temporal intensity profiles and calculate diffusivity values, respectively. The confocal fluorescent images in Fig. 3c illustrate the diffusion of the 50 nm (red) and 120 nm (green) nanoparticles along the collagen (I) matrix channel before and after PTT treatment. The red/green colors are meant to distinguish between 50 nm and 120 nm nanoparticles and not indicative of actual emission channel. The diffusion direction is from left (high concentration) to right (low concentration) at the same time point and the position for each particle size. Regardless of nanoparticle size, in untreated collagen (I) matrix, the average intensity along the channel length is low and most of the nanoparticles are populated at the left end of the channel whereas in a photo-thermally treated (PTT) collagen (I) matrix, we detected higher average fluorescence intensity through the entire length of the channel. Qualitatively, we can make two conclusions. (1) At a defined time t, the number of nanoparticles along the length of the channel is higher in PTT-treated channel for both nanoparticle sizes. (2) At the same nanoparticle concentration, the penetration depth through the collagen (I) matrix is increased when PTT is applied. This suggested that there was an increase in the diffusivity of nanoparticles through the collagen (I) matrix after PTT. We further scrutinized these results by developing intensity profile along the mid-channel for each particle size. Fig. 3d and e show temporal intensity profiles for the 50 nm nanoparticles in control and PTT-treated μ-channels, respectively. The PTT process increased the rate of intensity change compared to an intact collagen (I) matrix, regardless of the penetration depth. For a fixed penetration depth (same concentration gradient), the rate of increase in intensity can be a measure of how resistant the medium is against diffusion. For penetration depth of 0–500 μm, we calculated ~9 fold increase in the intensity rate for PTT treated channel. This means in PTT denatured collagen (I) matrix, 50 nm nanoparticles reached their initial local maximum concentration 9 times faster than intact collagen (I) matrix (control). We then plotted the normalized intensity *versus* penetration depth at t = 4 h which was the required time for x = 0 (Reference point)

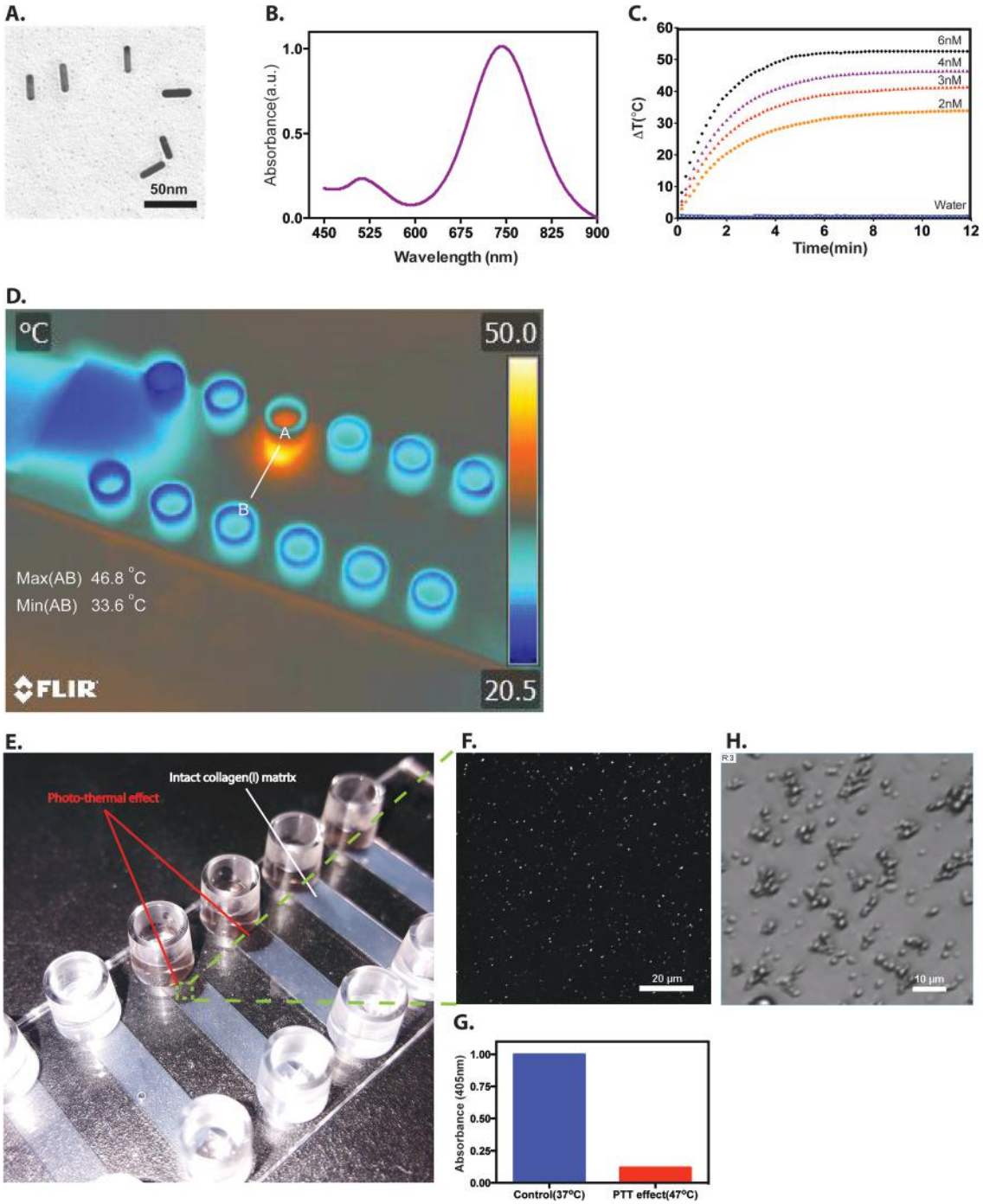

Fig. 2 Effect of photo-thermal GNRs on collagen (I) matrix. (A) Representative TEM image of gold nanorods with an aspect ratio of ~4. (B) Absorption spectrum of gold nanorods, which showed longitudinal and transverse plasmon peaks at 740 nm and 520 nm, respectively. (C) Photo-thermal characteristics of GNRs under fixed 3 W cm^{-2} laser power density as a function of concentration. (D) Thermographic image of the μ-chip during PTT process on GNRs injected into the channel. The GNR elevated the local channel temperature (red/yellow color) to an average of ~47 °C after raster illumination of laser beam (3 W cm^{-2}) over ~8 mm channel length for 6 min. (E) Optical image of the collagen μ-channels after PTT process. The collagen hydrogel appeared clear. (F) Reflectance confocal image of the channel after PTT. (G) Normalized absorption of collagen (I) hydrogel at 405 nm before and after PTT process. (H) Transmittance confocal image of the PTT affected channel area.

to reach its maximum point (Fig. 3f). For penetration depth of 100 μm–1000 μm, we found 2.1–18.0 fold raise in the intensity. We inferred in a PTT treated channel, the local concentration of 50 nm nanoparticles at different penetration depth was increased. Also, an increase in the intensity from 0% to 54% at $x = 1000$ μm suggests that the penetration depth in PTT-treated

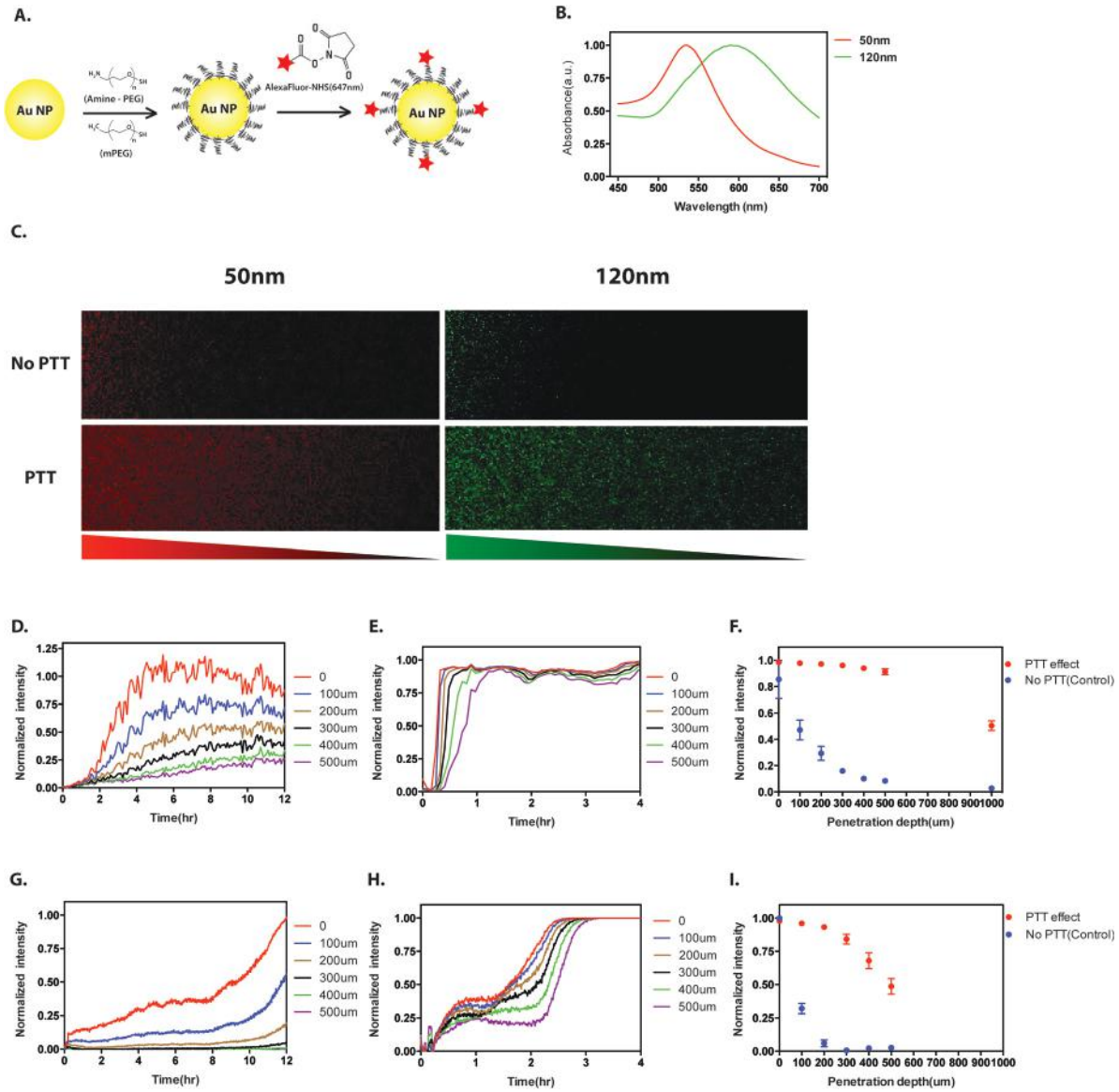

Fig. 3 Effect of Photo-thermal GNRs on diffusion inside collagen (I) matrix. (A) Schematic of the PEGylation and surface modification of gold nanoparticles with AlexFluor647 nm. (B) Absorption spectrum of fluorescent Alexafluor (647 nm)-conjugated gold nanoparticles. (C) Representative confocal images of two parallel channels with and without PTT process for 50 nm and 120 nm fluorescent-tagged gold nanoparticles. The red/green colors are meant to distinguish between 50 nm and 120 nm nanoparticles and not indicative of actual emission channel. (D) Mid-channel intensity profile for 50 nm without PTT. (E) Mid-channel intensity profile for 50 nm with PTT. (F) Penetration depth profile for 50 nm at t = 4 h with and without PTT. (G) Mid-channel intensity profile for 120 nm without PTT. (H) Mid-channel intensity profile for 120 nm with PTT. (I) Penetration depth profile for 120 nm at t = 2.5 h with and without PTT.

channel was increased. The effect of the PTT process for 120 nm particles followed the same trend as 50 nm nanoparticles, shown in Fig. 3g and h. 120 nm nanoparticles reached saturation in PTT-treated channel in ~3 h while in untreated channel the signal for the same spot started to saturate after 12 h. 120 nm nanoparticles showed fluorescent signals at 500 μm for PTT treat collagen (I) matrix as compared to untreated matrix. This suggested more than a 300 μm increase in penetration depth for 120 nm nanoparticles. We quantified the change in collagen (I) matrix diffusivity (D) by developing intensity profiles *versus* penetration distance at fixed time points and fitted the data to fick's law solution as described in equation 1:

$$C(x,t) = A\ erfc\left(\frac{x}{2\sqrt{Dt}}\right) \quad (1)$$

where C denotes nanoparticle intensity, x represents diffusion distance and t shows imaging time. Fig. 4 demonstrates the change in diffusivity of 50 nm and 120 nm inside the collagen (I) matrix after GNRs PTT effect. In the absence of PTT, 50 nm nanoparticles showed an effective diffusivity value of 1.62 ×

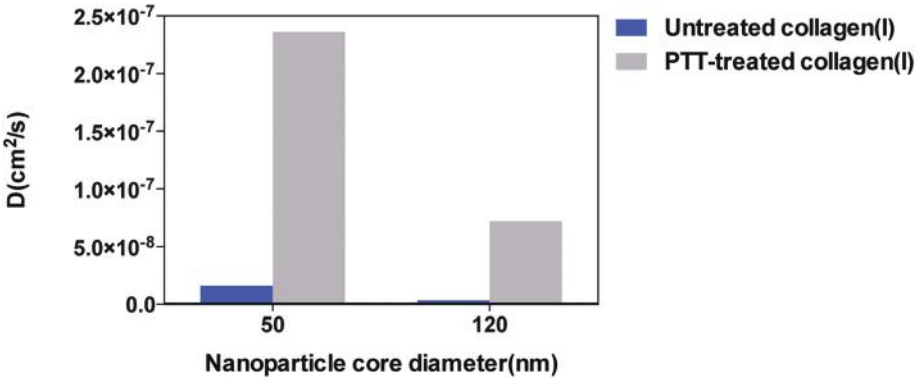

Fig. 4 Effect of GNRs PTT on the diffusivity of 50 nm and 120 nm gold nanoparticles inside collagen (I).

10^{-8} cm^2 s^{-1} through the collagen (I) matrix channel compared to 3.39×10^{-9} cm^2 s^{-1} for the 120 nm gold nanoparticles. Interestingly, PTT process increased the effective diffusivity of the 50 nm gold nanoparticle by ~14 fold (2.36×10^{-7} cm^2 s^{-1}) *versus* ~21 (7.22×10^{-8} cm^2 s^{-1}) fold for 120 nm nanoparticles. From this data, the diffusivity of the 120 nm nanoparticle becomes 4.5 times slower than the 50 nm inside collagen (I) matrix. Considering inverse proportionality of *D vs.* hydrodynamic radius in the Stokes–Einstein equation, a 2.4 times decrease in diffusivity based on core nanoparticle diameters is calculated. This discrepancy may be explained by a combination of different hydrodynamic radius after PEGylation/Dye conjugation and surface charge density between the 50 nm and 120 nm nanoparticles. Interestingly, we found that PTT process showed ~1.5 fold higher effect on diffusivity enhancement for 120 nm *versus* 50 nm. If one rules out average measurement errors and that PTT from GNRs homogeneously denatures collagen matrix, one would expect the same ratio of enhancement in diffusivity for both nanoparticle sizes. However, from Stokes–Einstein equation, D is inversely proportional to the term μR, where μ is medium viscosity and R is hydrodynamic radius. This suggests that the PTT effect from GNRs may inhomogeneously denature collagen fibers inside its network. This is supported by our earlier data that random coiled microstructures were detected at the bottom of the channel, suggesting that inhomogeneous viscosity appears inside the denatured collagen (I) matrix. So, what does this mean in terms of nanotherapeutic delivery to tumor cells? Larger nanoparticles such as the 120 nm can carry more therapeutic agents to cancer cells than smaller nanoparticles but previous studies have shown that these larger nanoparticles typically reside near the tumor vasculature. There could be a trade-off between the diffusivity of smaller nanoparticles through the tumor extracellular matrix *versus* the larger nanoparticles. Here, we showed the transport limitations of a larger nanoparticle can be negated by thermally denaturing the collagen (I) matrix first, which can potentially remove the barrier for transport of larger nanoparticles to tumor cells.

In conclusion, we used an *in vitro* model to show that a 2-step process can enhance the penetration of nanoparticles transport within a collagen matrix. The first step requires the denaturation of collagen structure by using gold nanorods heating, which effectively opens up the collagen (I) matrix for larger nanoparticles to transport through. We clearly showed a deeper penetration depth for 50 and 120 nm spherical gold nanoparticles within the collagen (I) matrix after gold nanorod priming. Further experiments will require the confirmation of improved transport of larger nanoparticles through the tumor matrix in animal models. The tumor extracellular matrix may prevent the transport of nanoparticles to the targeted tumor cells and the use of gold nanorods heating may prime the tumor for the "actual" nanoparticle therapeutic or diagnostic formulation to be successfully delivered to the tumor cells. This may be the case for both direction injection of "second" nanoparticles into tumors as well as *via* a systemic injection, where nanoparticles may have to diffuse through the matrix to reach the targeted cells. The gold nanorods may be introduced into the tumor *via* direct or systemic injection. *In vivo*, even if these gold nanorods do not penetrate deeply, the ability to heat and denature the localized tumor matrix may allow more of the subsequent or secondary nanoparticles to diffuse through. The incorporation of heat-generating components that denatures the tumor extracellular matrix may allow entire nanosystems to be transported through the tumor extracellular matrix and achieve specific tumor cell targeting.

Acknowledgements

WCWC would also like to acknowledge the Canadian Institute of Health Research (MOP-130143 and RMF-111623), Natural Sciences and Engineering Research Council (2015-06397), Prostate Cancer Canada (D2014-12) for supporting his research program.

References

1 R. K. Jain and T. Stylianopoulos, *Nat. Rev. Clin. Oncol.*, 2010, **7**, 653–664.
2 E. Ruoslahti, S. N. Bhatia and M. J. Sailor, *J. Cell Biol.*, 2010, **188**, 759–768.

3 W. Jiang, B. Y. Kim, J. T. Rutka and W. C. Chan, *Expert Opin. Drug Delivery*, 2007, **4**, 621–633.
4 J. V. Jokerst, T. Lobovkina, R. N. Zare and S. S. Gambhir, *Nanomedicine*, 2011, **6**, 715–728.
5 V. P. Zharov and D. O. Lapotko, *IEEE J. Sel. Top. Quantum Electron.*, 2005, **11**, 733–751.
6 L. Y. T. Chou and W. C. W. Chan, *Adv. Healthcare Mater.*, 2012, **1**, 714–721.
7 L. Zhang, F. Gu, J. Chan, A. Wang, R. Langer and O. Farokhzad, *Clin. Pharmacol. Ther.*, 2007, **83**, 761–769.
8 J. Hrkach, D. Von Hoff, M. M. Ali, E. Andrianova, J. Auer, T. Campbell, D. De Witt, M. Figa, M. Figueiredo, A. Horhota, S. Low, K. McDonnell, E. Peeke, B. Retnarajan, A. Sabnis, E. Schnipper, J. J. Song, Y. H. Song, J. Summa, D. Tompsett, G. Troiano, T. Van Geen Hoven, J. Wright, P. LoRusso, P. W. Kantoff, N. H. Bander, C. Sweeney, O. C. Farokhzad, R. Langer and S. Zale, *Sci. Transl. Med.*, 2012, **4**, 128ra39–128ra39.
9 C. J. Langer, M. A. Socinski and K. J. O'Byrne, *Proc. Am. Soc. Clin. Oncol.*, 2005, **23**(suppl 16), LBA7011.
10 D. Yoo, H. Jeong, C. Preihs, J.-S. Choi, T.-H. Shin, J. L. Sessler and J. Cheon, *Angew. Chem., Int. Ed.*, 2012, **51**, 12482–12485.
11 A. P. R. Johnston, M. M. J. Kamphuis, G. K. Such, A. M. Scott, E. C. Nice, J. K. Heath and F. Caruso, *ACS Nano*, 2012, **6**, 6667–6674.
12 T. A. ElBayoumi and V. P. Torchilin, *Clin. Cancer Res.*, 2009, **15**, 1973–1980.
13 M. E. Davis, Z. G. Chen and D. M. Shin, *Nat. Rev. Drug Discovery*, 2008, **7**, 771–782.
14 C. J. Cheng, G. T. Tietjen, J. K. Saucier-Sawyer and W. M. Saltzman, *Nat. Rev. Drug Discovery*, 2015, **14**, 239–247.
15 S. D. Perrault, C. Walkey, T. Jennings, H. C. Fischer and W. C. W. Chan, *Nano Lett.*, 2009, **9**, 1909–1915.
16 Y.-L. Yang, S. Motte and L. J. Kaufman, *Biomaterials*, 2010, **31**, 5678–5688.
17 P. A. Netti, D. A. Berk, M. A. Swartz, A. J. Grodzinsky and R. K. Jain, *Cancer Res.*, 2000, **60**, 2497–2503.
18 S. Ramanujan, A. Pluen, T. D. McKee, E. B. Brown, Y. Boucher and R. K. Jain, *Biophys. J.*, 2002, **83**, 1650–1660.
19 O. Tredan, C. M. Galmarini, K. Patel and I. F. Tannock, *JNCI, J. Natl. Cancer Inst.*, 2007, **99**, 1441–1454.
20 A. Pluen, Y. Boucher, S. Ramanujan, T. D. McKee, T. Gohongi, E. di Tomaso, E. B. Brown, Y. Izumi, R. B. Campbell, D. A. Berk and R. K. Jain, *Proc. Natl. Acad. Sci. U. S. A.*, 2001, **98**, 4628–4633.
21 L. T. Baxter and R. K. Jain, *Microvasc. Res.*, 1989, **37**, 77–104.
22 E. A. Sykes, J. Chen, G. Zheng and W. C. W. Chan, *ACS Nano*, 2014, **8**, 5696–5706.
23 E. Huynh and G. Zheng, *WIREs Nanomed. Nanobiotechnol.*, 2013, **5**, 250–265.
24 S. Kunjachan, R. Pola, F. Gremse, B. Theek, J. Ehling, D. Moeckel, B. Hermanns-Sachweh, M. Pechar, K. Ulbrich, W. E. Hennink, G. Storm, W. Lederle, F. Kiessling and T. Lammers, *Nano Lett.*, 2014, **14**, 972–981.
25 D. B. Kirpotin, *Cancer Res.*, 2006, **66**, 6732–6740.
26 M. Magzoub, S. Jin and A. S. Verkman, *FASEB J.*, 2007, **22**, 276–284.
27 T. T. Goodman, P. L. Olive and S. H. Pun, *Int. J. Nanomed.*, 2007, **2**, 265–274.
28 S. Murty, T. Gilliland, P. Qiao, T. Tabtieng, E. Higbee, A. A. Zaki, E. Puré and A. Tsourkas, *Part. Part. Syst. Charact.*, 2014, **31**, 1307–1312.
29 S. J. Kuhn, S. K. Finch, D. E. Hallahan and T. D. Giorgio, *Nano Lett.*, 2006, **6**, 306–312.
30 C. Wong, T. Stylianopoulos, J. Cui, J. Martin, V. P. Chauhan, W. Jiang, Z. Popovic, R. K. Jain, M. G. Bawendi and D. Fukumura, *Proc. Natl. Acad. Sci. U. S. A.*, 2011, **108**, 2426–2431.
31 R. K. Jain, *J. Clin. Oncol.*, 2013, **31**, 2205–2218.
32 M. R. Villegas, A. Baeza and M. Vallet Regí, *ACS Appl. Mater. Interfaces*, 2015, 151013114646000.
33 F. Tewes, E. Munnier, B. Antoon, L. Ngaboni Okassa, S. Cohen-Jonathan, H. Marchais, L. Douziech-Eyrolles, M. Soucé, P. Dubois and I. Chourpa, *Eur. J. Pharm. Biopharm.*, 2007, **66**, 488–492.
34 A. P. Esser-Kahn, S. A. Odom, N. R. Sottos, S. R. White and J. S. Moore, *Macromolecules*, 2011, **44**, 5539–5553.
35 R. K. J. S. R. Chary, *Proc. Natl. Acad. Sci. U. S. A.*, 1989, **86**, 5385–5385.
36 Z. Qin and J. C. Bischof, *Chem. Soc. Rev.*, 2012, **41**, 1191.
37 C. Ungureanu, R. Kroes, W. Petersen, T. A. M. Groothuis, F. Ungureanu, H. Janssen, F. W. B. van Leeuwen, R. P. H. Kooyman, S. Manohar and T. G. van Leeuwen, *Nano Lett.*, 2011, **11**, 1887–1894.
38 T. B. Huff, M. N. Hansen, Y. Zhao, J.-X. Cheng and A. Wei, *Langmuir*, 2007, **23**, 1596–1599.
39 W.-S. Kuo, C.-N. Chang, Y.-T. Chang, M.-H. Yang, Y.-H. Chien, S.-J. Chen and C.-S. Yeh, *Angew. Chem., Int. Ed.*, 2010, **49**, 1–6.
40 T. B. Huff, L. Tong, Y. Zhao, M. N. Hansen, J.-X. Cheng and A. Wei, *Nanomedicine*, 2007, **2**, 125–132.
41 T. S. Hauck, T. L. Jennings, T. Yatsenko, J. C. Kumaradas and W. C. W. Chan, *Adv. Mater.*, 2008, **20**, 3832–3838.
42 K. C. Hribar, M. H. Lee, D. Lee and J. A. Burdick, *ACS Nano*, 2011, **5**, 2948–2956.
43 D. Wang, Z. Xu, H. Yu, X. Chen, B. Feng, Z. Cui, B. Lin, Q. Yin, Z. Zhang, C. Chen, J. Wang, W. Zhang and Y. Li, *Biomaterials*, 2014, **35**, 8374–8384.
44 S. Ramanujan, A. Pluen, T. D. McKee, E. B. Brown, Y. Boucher and R. K. Jain, *Biophys. J.*, 2002, **83**, 1650–1660.
45 N. R. Jana, *Small*, 2005, **1**, 875–882.
46 C. A. Miles and A. J. Bailey, *Proc. – Indian Acad. Sci., Chem. Sci.*, 1999, **111**, 71–80.
47 L. Bozec and M. Odlyha, *Biophys. J.*, 2011, **101**, 228–236.
48 A. O. Brightman, B. P. Rajwa, J. E. Sturgis, M. E. McCallister, J. P. Robinson and S. L. Voytik-Harbin, *Biopolymers*, 2000, **54**, 222–234.
49 N. T. Wright and J. D. Humphrey, *Annu. Rev. Biomed. Eng.*, 2002, **4**, 109–128.

